Device

Article

# Squishy bioelectronic circuits

## Graphical abstract

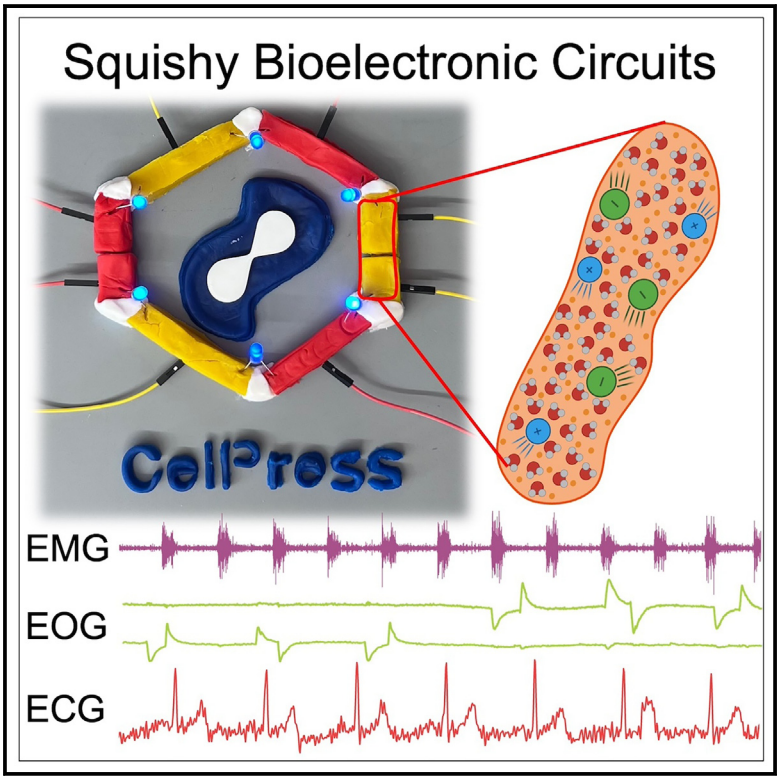


## Highlights

- Squishy circuits provide low-cost bioelectronic interface solutions
- Comparable performance to traditional bioelectronic systems
- Self-healing properties enhance durability
- Effective in EEG, ECG, EMG, and EOG applications

## Authors

Alexandra Katsoulakis, Favour Nakyazze, Max Mchugh, Sean Morris, Monil Bhavsar, Om Tank, Dmitry Kireev

## Correspondence

dkireev@umass.edu

## In brief

We present here squishy circuits, innovative bioelectronic wearables made from affordable household materials. These circuits close the gap between expensive medical devices and accessible health tools, offering a new approach to wearable health monitoring. They can effectively measure brain, heart, muscle, and eye activity, with performance similar to traditional systems. Their self-healing properties and sensitivity to temperature make them durable, bringing advanced health monitoring within reach for the general population.


**Develop**
Prototype with demonstrated applications in relevant environment

Katsoulakis et al., 2025, Device *3*, 100553
January 17, 2025 
Published by Elsevier Inc.
https://doi.org/10.1016/j.device.2024.100553

CellPress

Device

CellPress
OPEN ACCESS

Article

# Squishy bioelectronic circuits

Alexandra Katsoulakis,[1,2] Favour Nakyazze,[1,2] Max Mchugh,[1,2] Sean Morris,[1,2] Monil Bhavsar,[1] Om Tank,[1] and Dmitry Kireev[1,3,*]

[1]Department of Biomedical Engineering, University of Massachusetts Amherst, Amherst, MA, USA
[2]These authors contributed equally
[3]Lead contact
*Correspondence: dkireev@umass.edu
https://doi.org/10.1016/j.device.2024.100553

**THE BIGGER PICTURE** We show that squishy circuits (SCs) exhibit a transformative shift in the design and application of bioelectronic devices. SCs, made of simple, inexpensive household materials, effectively bridge the gap between costly medical technology and accessible educational tools. This convergence represents a frontier era of wearable technology that is both cost effective and highly functional, thus broadening the accessibility of advanced healthcare monitoring to wider populations. Our research demonstrates that SCs can effectively measure various biopotentials, including cardiac, neural, muscular, and ocular activity. Intriguingly, these SCs possess self-healing properties and are sensitive to temperature variations. This approach democratizes health monitoring by making it more affordable and accessible.

## SUMMARY

In the pursuit of advancing wearable bioelectronics, our study introduces Squishy Circuits (SCs) as a promising low-cost biointerface electrode material, particularly for electrophysiological applications. Addressing the essential need for low-impedance interfaces in electrophysiological measurements, we explore the conductivity and resistance of various SCs and put them to the test against classical bioelectronic systems. Notably, SCs exhibit self-healing properties that enhance their durability and functionality. Electrochemically, SCs show normalized impedance (at 1 kHz) of $3.4 \pm 0.6\ k\Omega$, which is 4 times lower (better) compared to that of copper and 10 times lower compared to Ag/AgCl gel electrodes. Our findings demonstrate that SCs are a viable and effective alternative for wearable electrophysiology, such as monitoring the brain and cardiac activities, with signal-to-noise ratios up to 115, while being simple to produce and apply. This study highlights the potential of SCs to revolutionize wearable bioelectronics by offering an affordable, robust, and user-friendly biointerface electrode material.

## INTRODUCTION

The field of bioelectronics, particularly wearable bioelectronics, is rapidly evolving, driven by advancements in materials science and manufacturing techniques. These devices are becoming increasingly accessible, broadening their application in non-invasive health monitoring and making a significant impact on the field.[1–6] With their accessibility and utilization on the rise, they are expanding their reach to a broader audience and optimizing their functionality for maximum benefit.[7,8] Wearable bioelectronics are engineered to capture a variety of physiological signals, such as those from electroencephalography (EEG; brain activity), electromyography (EMG; muscle activity), electrocardiography (ECG; heart activity), and electrooculography (EOG; ocular activity), through biocompatible sensor arrays that include strain sensors,[9] temperature sensors,[10] and electrophysiological sensors,[11] among others. The functionality of these devices is enhanced by their ability to operate within low-noise environments, thus ensuring accurate measurements critical for effective monitoring.[12]

A crucial aspect of wearable bioelectronics is the selection of materials used in their construction.[7] The spectrum ranges from conventional conductive metals to innovative nanostructures like carbon nanotubes,[13] graphene,[14] silver nanowires,[15] and organic polymers,[16] among others. These materials are selected for their beneficial electrical properties, such as high conductivity, which is essential for maintaining the efficiency of electrophysiological measurements.[17,18] However, these materials also present challenges in terms of costly precursor sources, handling, fabrication, and durability.[17,18] Traditional processing techniques such as photolithography and modern methods like inkjet printing and electrospinning are employed to structure these materials into functional designs, somewhat restricting their employment in broad use.[5]

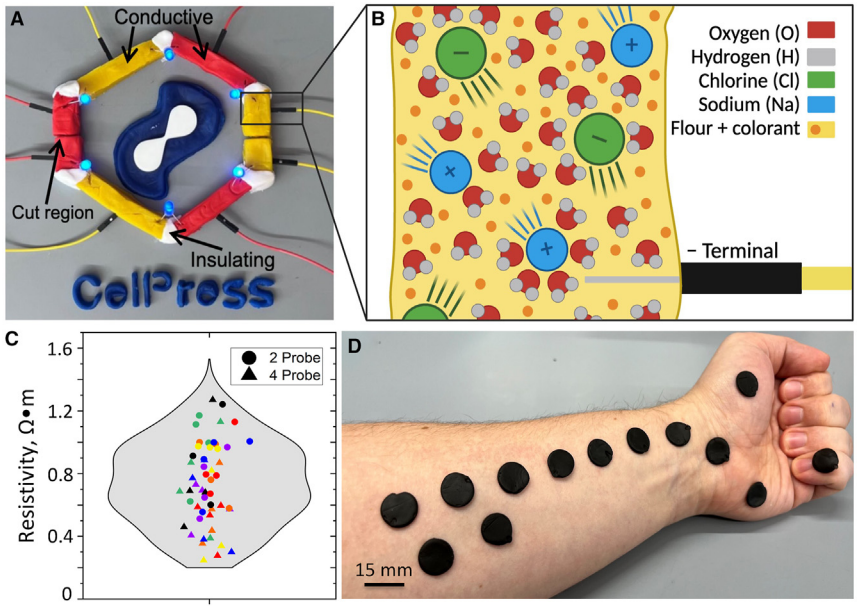


**Figure 1. Electrical properties of the SCs**

(A) Photograph of the Squishy Circuits (SCs) arranged into a hexagon with a series of conductive (colored) and insulating (white) dough, connected to a power supply and a series of LEDs.

(B) Schematic representation of the ionic flow within conductive SCs. The dough, composed of mainly salt (NaCl) and water, enables electrical conductivity. Sodium ions ($Na^+$) migrate toward the negative terminal, while chloride ions ($Cl^-$) move toward the positive terminal, with water and flour molecules uniformly distributed throughout.

(C) Statistical distribution of the SC resistivity values, with each color ($N = 3$ for each color, $N = 21$ total) corresponding to an SC of the same color. As one can see, color itself does not affect the performance of conductive SCs.

(D) Photograph of an array of SCs arranged on a human arm before electrophysiological measurements.

In this context, here we explore the potential of using everyday materials, made from common household items. These materials not only offer an educational tool but have also proven to be effective in creating wearable circuits and bioelectronic electrodes due to their conductive and insulative properties. Their simplicity and the familiarity of these materials could revolutionize the way wearable bioelectronics are perceived and interacted with by users.

Previously, only a handful of works have approached making high-quality bioelectronic devices using household materials. Xu et al., for example, developed pencil-drawn electronics, relying on conductive properties of the graphite that makes the pencil rod.[19] They made cost-effective and disposable on-skin electronic devices as biophysical sensors, sweat biochemical sensors, thermal stimulators, and humidity energy harvesters. Their fabrication method, however, requires a rather uncontrollable number of pencils rubbing together to make the conductive electrodes.[19] Notable is the work of Ershad et al., who utilized common office pens and filled them with conductive nanomaterial inks as a way to distribute the inks onto the skin.[20,21] The inks, however, are made of organic conductive polymers, which are not entirely household available, and require proper chemical handling prior to on-skin use. The work of Zhang et al. reports on MXene-infused conductive hydrogels as strain sensors that are highly sensitive, stretchable, capable of adhering to arbitrary complex surfaces, and self-healable.[22] They do show stretchability, self-healing ability, tissue conformability, and adhesiveness to various surfaces like human skin but were only tested with mechanical properties like strain, compressive, and tensile tests without electrochemical or wearable impedance testing. The work of Zou et al. reports on a complex e-skin made of silver nanoparticles infused polyimine that has mechanical and electrical properties that allow for it to be used in temperature-related sensors.[23] The e-skin is malleable and recycled so that it can be manipulated mainly at low temperatures. However, they do not report on the electrochemical or impedance properties of their materials.

In this work, we used a commercially available, low-cost child educational toy Squishy Circuits (SCs; see Figure 1). SCs, which are made from household materials like flour and salt, have shown promise as practical and efficient educational tools for kids. As shown in the experimental procedures, we use the commercially pre-made SC dough, but the full fabrication protocol can be found in Peppler et al.[24] and Conductive Play Dough – Salt Dough Recipe.[25] Here, we demonstrate that conductive SC dough can be used as practical and highly efficient wearable circuits and bioelectronic electrodes due to its conductive and insulative properties. We report comprehensively on the electrochemical, electrical, and electrophysiological properties of the SCs. We successfully made biopotential sensing electrodes using SCs and rigorously characterized their interface impedance to skin (on both human and porcine skin). The successful applications include EEG, ECG, EMG, and EOG. Interestingly, by the nature of the conductive putty, it is intrinsically self-healing, enabling robust interfacing with the human skin. Moreover, we show that the SCs can be used to reliably sense temperature. As one can see from Figure 1, these SCs can be easily assembled into complex conductive/insulating structures and placed on human skin (see more pictures in Figure S1).

## RESULTS AND DISCUSSION

### SC conductivity

The first major property of merit for wearable electrodes is their conductivity. Two-probe and four-probe resistance measurement techniques were used to measure the SCs' performance. For this purpose, the SCs were formed into a 3D-printed mold with dimensions of 5 × 60 × 1 mm, ensuring consistent dimensions for each measurement. Conductive tape was affixed to both ends of the mold to provide a stable interface for the

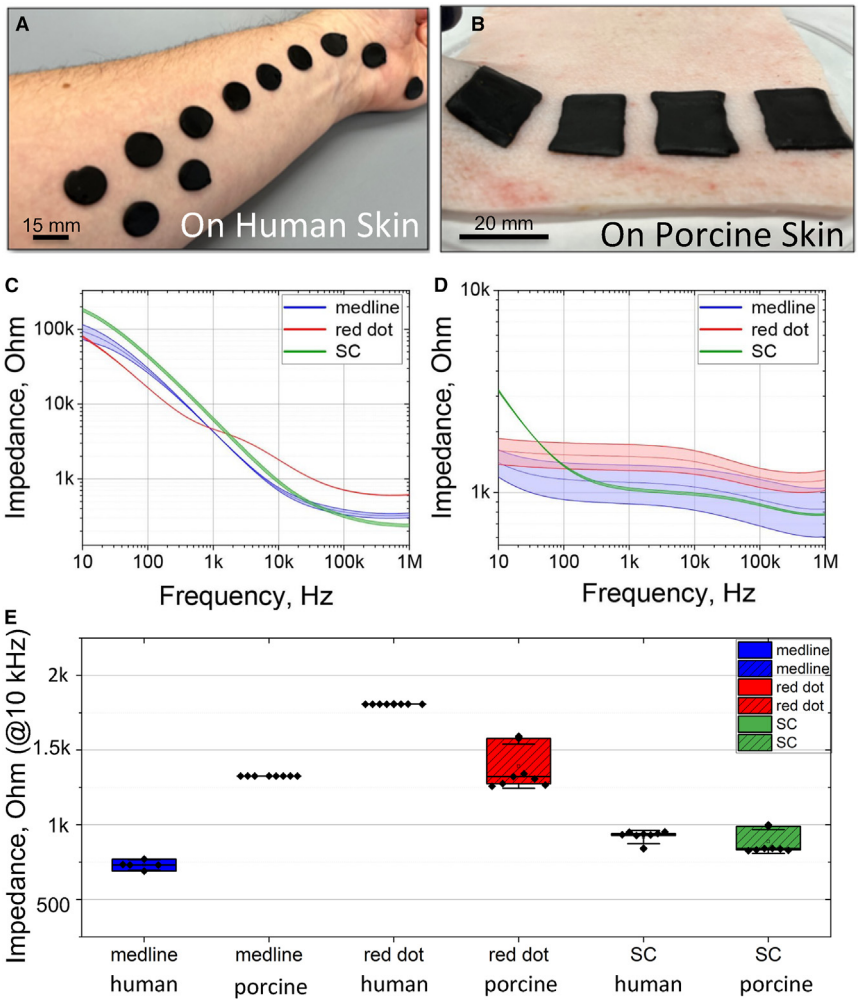


**Figure 2. Wearable operation and interface impedance of the SCs**

(A) Optical photograph of the SCs used as wearable electrode on human skin. Scale bar: 15 mm.

(B) Optical photograph of the SCs used as wearable electrode on porcine skin. Scale bar: 20 mm.

(C and D) Direct comparison of the 2-probe impedance of the SCs (green), Red Dot (red), and Medline (blue) on two types of skin: (C) human skin and (D) porcine skin (explant). Each plot shows a mean line (dark solid line) and standard deviation (colored cloud) from $N = 3$ samples of each kind.

(E) Statistical comparison of the three different electrodes' impedance (2 probe, measured @10 kHz). The box represents 25% and 75% with a mean; outliers are ±SD.

probes. 2-Probe resistance and 4-probe resistance were then measured using a Keysight B2902B precision source/measure unit. $N = 3$ samples of each color were tested, and the results can be seen in Figure 1C. It was found that the average resistivity values of the 4-probe data were measured to be slightly lower than those of the 2-probe data. The average resistivity observed during 4-probe measurements was 0.61 ± 0.25 Ω m, whereas the 2-probe measurement average was 0.89 ± 0.21 Ω m. Although the resistivity of the SC dough is significantly higher compared to that of copper, it is not a major drawback for creating wearable electrodes for electrophysiology. The electrode-to-skin interface impedance takes precedence in this case, and since the SCs are soft and pliable, they conform to the micro-curvature of the skin, forming a perfectly conformal interface, establishing superior interface to the skin.

## Skin impedance

To understand the effectiveness of squishy bioelectronic circuits as wearable interfaces, we analyzed the effectiveness of the bioelectronic interface between the electrode and skin—the impedance. To see a complete picture, skin impedance measurements were performed with both 2-probe and 4-probe impedance configurations for the SCs as well as two types of Ag/AgCl gel electrodes: 3M Red Dot and Medline MedGel. Furthermore, the skin impedance was measured on both human skin and porcine skin—two commonly used models. Optical images of the SCs on human and porcine skin can be seen in Figures 2A and 2B.

It is known that electrode dimensions play an important role in electrode-skin impedance, as the classical electrical circuit model states that electrode-skin impedance is inversely proportional to the area of the electrode. Therefore, to have a rigorous and fair comparison, all electrodes were prepared with equal dimensions (25 × 20 mm, or ∼500 $mm^2$). These dimensions were chosen to match the conductive area of the standard gel electrodes to which the SCs were being compared. Since SCs do not naturally strongly self-adhere to human or porcine skin, the interface was supplemented by placing the electrodes on 3M Micropore Silicone Tape, creating a multi-use SC tattoo (see Figure S1). The tattoo was then placed on the subject where the tape would adhere to the skin, forcing contact between the tattoo and the skin to allow electrical signals to be obtained and read from the SCs.

As seen in Figures 2C and 2D, SCs perform on par with the commercial state-of-the-art gel electrodes when measured via 2-probe impedance testing. The shapes of the impedance curves of both gel electrodes and the SC tattoos are similar during both porcine and human skin testing. A slight increase in impedance in the SCs during porcine testing compared to gel electrodes was seen at lower frequencies (<100 Hz). This can be explained by the slightly weaker adhesion of the SC compared to the gel electrodes causing poor contact between the SC and the porcine skin. However, a higher signal current overcame this contact issue.

A common figure of merit regarding skin impedance is the value measured at 10 kHz. At this frequency, the signal will pass through both intra- and extracellular fluids, giving a strong

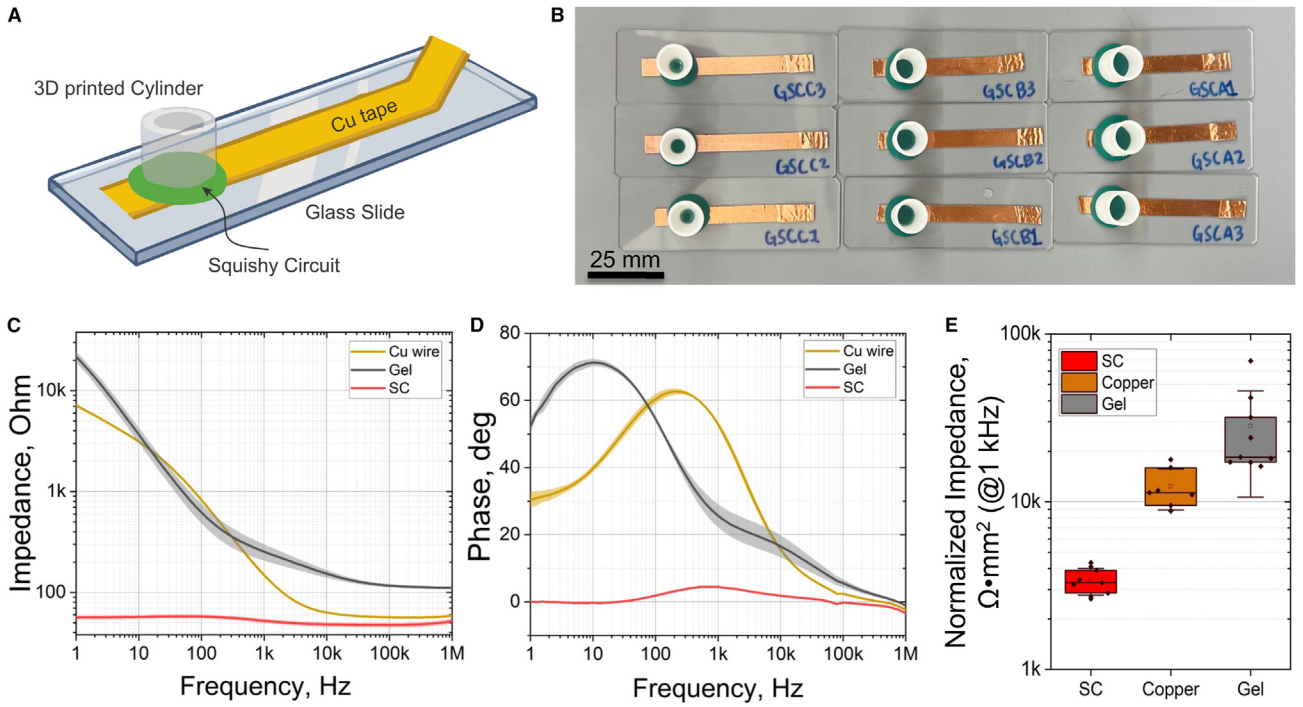


**Figure 3. Electrochemical properties of the SCs**

(A) Schematic design of the SCs during EIS measurements.

(B) Optical photograph of the array of $N = 9$ SCs with three different electrode openings.

(C) Impedance plot of the SCs (red), copper electrodes (dark orange), and gel electrodes (gray) with an electrode diameter of 10 mm.

(D) Phase plot of the SCs (red), copper electrodes (dark orange), and gel electrodes (gray) with an electrode diameter of 10 mm.

(E) Statistical comparison of normalized impedance values for SCs (red), copper electrodes (dark orange), and gel electrodes (gray) with diameters of 5, 7.5, and 10 mm. Impedance values were normalized based on the electrode areas. The box reprsents 25% and 75% with a mean; outliers are ±SD.

indication of tissue impedance.[26–28] As seen in Figures 2C and 2D, for both porcine and human skin, the SC skin impedance measured was ~1 kΩ, while the Ag/AgCl electrodes (Medline and Red Dot) measured were ~1 and ~2 kΩ, respectively. Additionally, as shown in Figures 2C and 2D, a major difference from the 2-probe interface impedance measured on human and porcine skin was observed: the impedance measured on human skin compared to porcine skin is much higher at lower frequencies (<10 kHz). At or above the 10 kHz frequency, however, the skin impedances measured for human skin and porcine skin are relatively similar, suggesting that 10 kHz or above will be the best set point when comparing electrode performance on both skin models (see results in Figure S2). Overall, as one can see from Figure 2E, the SCs feature interface impedance that is lower (better) than the state-of-the-art Red Dot gel elctrodes and perform on par with the Medline gel eleectrodes.

While the 2-probe testing provides an important figure of merit to qualify electrophysiology measurements, 4-probe bioimpedance is another modality that is essential for complex wearable systems.[26,29,30] This setup involves separating the injection and sensing electrodes, bypassing the interface impedance, and directly measuring the tissue impedance; hence, the 4-probe impedance values are expected to not vary significantly between electrodes. Our hypothesis holds rather well, as one can see from Figures S3 and S4, as there is little difference between the impedance readings of each electrode. When measuring at 10 kHz on human skin, the skin impedances of Medline, Red Dot, and SC electrodes averaged 44, 39, and 17 Ω, respectively. At the same current on porcine skin, the skin impedances of each electrode averaged 400, 195, and 330 Ω. A difference of one order of magnitude can be observed between the skin impedances on porcine skin versus human skin. This difference can be explained by the 4-probe configuration and skin difference. Specifically looking at the difference between the skin models, skin on a living human has a higher moisture content than the thawed porcine skin being tested. An increase in moisture content leads to an increase in conductivity, leading to lower impedance, a concept that was observed in the data.

## Electrochemical impedance

In addition to measuring skin impedance, we performed electrochemical impedance spectroscopy (EIS) to evaluate the electrochemical impedance of the SCs. During the experimental procedures, SC tattoos samples and control samples were placed on a glass slide, using copper tape as an interconnect (see Figure 3A). To test the EIS, we used 3D-printed cylinders with varying diameters (10, 7.5, and 5 mm; see Figure 3B and experimental procedures for details) to test the samples over different areas. After EIS measurements, we fitted the data to

an equivalent circuit and extracted the impedance at 1 kHz. We used a characteristic frequency of 1 kHz according to community standards.[31,32] The impedance and phase diagrams can be found in Figures 3C and 3D for SCs in direct comparison to control electrodes: copper tape and Ag/AgCl gel electrodes (3M Red Dot). The SC tattoos exhibit much lower impedance across the entire frequency spectrum. The phase values of the SCs ranged from $-5^{\circ}$ to $5^{\circ}$, indicating a highly resistive interface, whereas the gel and copper tape electrodes were significantly more capacitive. Figure S5 provides a detailed analysis of these electrodes made with different areas. The impedances normalized to the electrode area are shown in Figure 3E, with normalization performed by multiplying the electrode area by the impedance. The SC tattoos demonstrate the best electrochemical performance with the lowest normalized impedance (measured at 1 kHz) at $3.4 \pm 0.6$ k$\Omega$ mm$^2$. In comparison, the copper tape electrode shows a normalized impedance (@ 1 kHz) of $11.3 \pm 3.2$ k$\Omega$ mm$^2$, an $\sim$3-fold increase in normalized impedance compared to the SC. The normalized impedance of the gel electrode was even higher at $28.2 \pm 17.6$ k$\Omega$ mm$^2$. These findings underscore the superior effectiveness of the SC electrodes in minimizing electrode impedance compared to both copper tape and Ag/AgCl gel electrodes. Reducing impedance is a crucial objective in bioelectronic systems and electrodes due to its impact on measurement sensitivity, noise reduction, and overall performance. We expect that the SC tattoos will perform as well as gel electrodes when utilizing skin-adhering electrodes.

To verify the accuracy of our experimental setup with the SC electrodes and address the potential for ion leaching, we measured the conductivity of the phosphate buffered saline (PBS) solution before and after the EIS measurements. The average conductivity of the PBS solution before EIS measurements was $15.49 \pm 0.50$ mS/cm. After, it was measured that the average conductivity increased to $19.06 \pm 0.45$ mS/cm. This increase in conductivity suggests that some ions may have leached from the SCs into the PBS solution. However, the increase in ionic concentration within the PBS solution should not significantly affect the impedance of the SC electrodes themselves.

## Electrophysiology measurements

To evaluate the real-time applicability of SCs as tattoo-like wearables, electrophysiological measurements were conducted utilizing SCs alongside state-of-the-art Ag/AgCl gel electrodes. The gel electrodes employed as benchmarks were the Cardinal Health Kendall 5400 Diagnostic Tab Electrodes. SCs were placed on top of a medical-grade tape with copper lead-out wires for electrical interconnects (see experimental procedures for details). All electrophysiological data were acquired using OpenBCI's Ganglion board, while post-processing was accomplished via MATLAB. The EEG, ECG, EMG, and EOG measurement setups and electrode placements are shown in detail in Figure S6.

To get into the electrical dynamics of the brain, EEG technology emerges as a pivotal tool, offering a comprehensive visualization of these neural signals. In the pursuit of EEG signal acquisition, an arrangement involving the placement of two electrodes on the subject's forehead, precisely the Fp1 and Fp2 positions within the 10–20 EEG system, was utilized. These electrodes were sampled independently, with a common reference electrode (RE) placed on one of the subject's earlobes. EEG traces spanning a duration of between 320 and 360 s were recorded. The subject followed a set protocol where they kept their eyes open for half of the recording and then closed for the second half. The recorded EEG data underwent analysis through a short-time Fourier transformation (STFT), which allowed for the generation of a heatmap depicting signal frequencies alongside their corresponding power levels, measured in dB (Figure 4A). It has been established that EEG signals taken while the subject's eyes are closed exhibit prominent $\alpha$ waves (8–13 Hz), particularly when the electrodes from which the signals are taken are situated at the Fp1 and Fp2 positions. As evidenced by Figures 4A and S7, both the SCs and gel electrode spectrograms illustrated higher power levels across the 8–13 Hz spectrum while the subject's eyes were closed. Hence, it can be concluded that SCs effectively capture EEG signals, thus affirming their suitability for demanding brainwave measurement applications.

For ECG recordings, two electrodes were positioned on opposing forearms. An RE was placed on an area of low electrical activity, such as the elbow. This arrangement was used to capture signals using gel electrodes and SCs, albeit at separate times, enabling direct comparative analysis. The ECG traces from both the SC tattoos and gel electrodes, depicted in Figure 4B, exhibit the distinct characteristic domains of ECG signals (P, Q, R, S, T). The signal power is higher for the SC readings compared to the gel electrode readings; however, the noise is also larger, resulting in a lower signal-to-noise ratio (SNR). The SNR for SCs was determined to be $82 \pm 24$, whereas the SNR for the Ag/AgCl gel electrodes was $96 \pm 21$. While the SNR for the SC tattoos is lower than that for the gel electrodes, a little noise does not detract from providing relevant signal shape and information.

In addition to assessing the SCs' capability to detect and replicate electrical signals from the heart, we conducted tests to evaluate the electrical stability of SCs following deformation. Given the malleable nature of the material, SCs can undergo deformation under pressure. Particularly, the shape of SC tattoos can alter due to these forces, resulting in a thinner and less uniform appearance. To assess the impact of deformation on the electrical properties of the tattoo, a series of measurements were taken before and after deformation using a set of tattoos. Deformation was achieved by pressing the tattoo firmly against the subject's arm using the thumb, causing the SC electrode to flatten. Images depicting the tattoo before and after deformation are presented in Figure S8. Post-deformation, measurements for the SC electrodes were $30 \times 30$ mm for the positive terminal electrode and $29 \times 29$ mm for the negative terminal electrode. However, neither maintained their original rectangular shape, instead exhibiting an amorphous form. ECG testing was conducted both before and after deformation following the same methodology as described earlier. Graphs of the signals measured can be found in Figure S8. Time traces from both tests exhibited typical ECG waveforms (P, Q, R, S, T), with consistent signal power across both tests. However, a minor amount of noise was observed from the deformed tattoo. The SNR values for both tests were determined, with the SNR for the undistorted tattoo measured at $115 \pm 49$, higher than the SNR of the deformed tattoo, which was found to be $99 \pm 35$. Notably, both SNR values

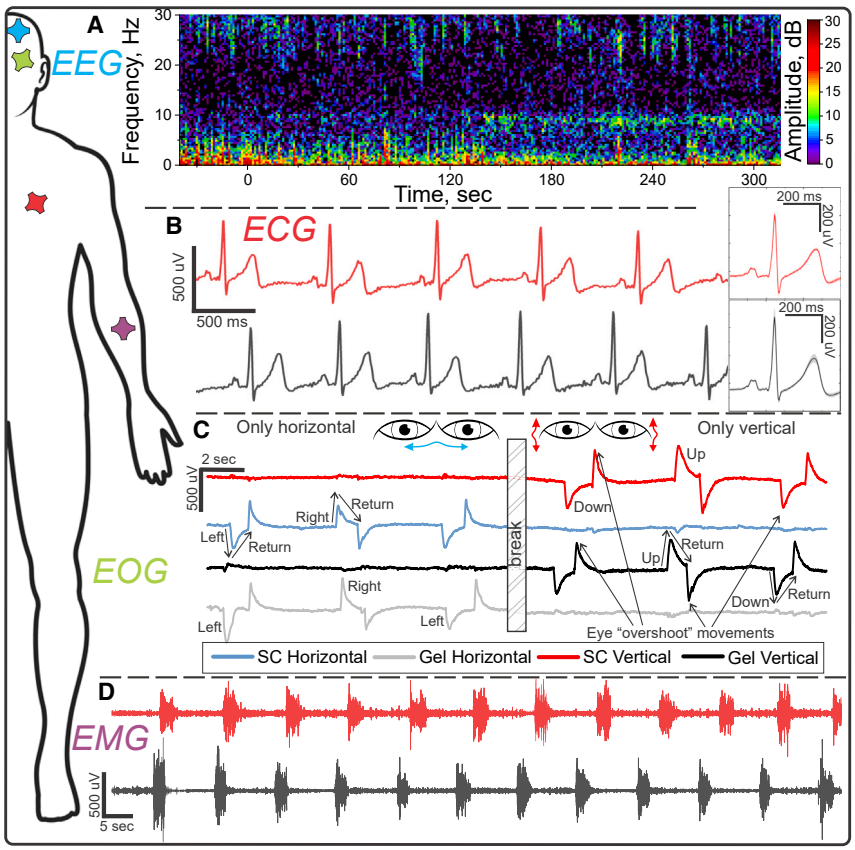


**Figure 4. Electrophysiology measurements with SCs shown from top to bottom**

(A) EEG spectrogram of an SC tattoo placed on the FP1 location on subject's forehead with the first 120 s in an eye-open state and the remaining time in an eye-closed state.

(B) 6 s ECG time trace (left) and average signal shape and amplitude (right) from SC tattoos (red) and Ag/AgCl gel electrodes (black). Cloud near average value is a standard deviation.

(C) EOG signals from differential channels recording horizontal and vertical ocular polarization in SC tattoos (blue, red) and gel electrodes (gray, black) during left-right eye movements (left) and up-down eye movements (right).

(D) EMG recording from subjects' forearm muscle contractions from SC tattoos and Ag/AgCl gel electrodes. Muscle contractions may be seen from the rapid increases in signal amplitude.

fell within one standard deviation of the average SNR recorded during initial ECG testing via SCs (82 ± 24), while significantly high standard deviations values are associated with (1) the normal variations of the recording quality during a few minutes of continuous recording and (2) the low sampling rate of the Ganglion board used to measure these signals. With only a sampling rate of 200 Hz, the max peaks from the ECG signals were not captured consistently, resulting in an ECG signal with high variability in the peaks of the ECG signals. From these findings, it can be inferred that while deformations to the tattoo caused by external forces have a slight impact on the noise of electrical readings, the overall capacity to accurately detect and reproduce electrical signals from the body remains largely unaffected by such deformations.

Next, a study was performed to determine their ability to maintain electrical performance during long-term exposure of the SCs to the human skin, as body moisture (e.g., sweat) may affect the electrode's performance. For the experiments, two SC tattoos were placed on opposite arms for ECG measurements as previously described. An Ag/AgCl electrode was also placed on the forearm to compare the SCs' biocompatibility with standard electrodes. All electrodes were left on the skin for 8 h, with ECG measurements taken from the SC tattoos periodically at 0, 2, 4, and 8 h. The ECG tests were conducted and analyzed as previously described (see Figure S9). The SNR for each signal was calculated to compare the electrical performance of the tattoo over time. The SNR was 82 ± 22 at 0 h, 49 ± 14 at 2 h, 95 ± 27 at 4 h, and 75 ± 25 at 8 h. These SNR values fall within one standard deviation of the original SNR measured with SC tattoos (82 ± 24), indicating that SCs maintain their electrical properties after long-term skin exposure. After 8 h, the electrodes were removed, and the skin was inspected, with no signs of irritation (Figure S9). One can see that after removing the SC tattoo at the end of the day, only slight indentations in the skin were seen, while the Red Dot electrode caused indentations and left gel residue. The SC electrodes were moister after 8 h of skin exposure compared to before application, likely due to the absorption of natural body liquids (i.e., sweat) that replenish any water lost from the SC due to evaporation. Only at 2 h was the SNR significantly lower than expected, a result that can be attributed to poor contact between the skin and tattoo. This issue was resolved by adding extra support by wrapping tape fully around the tattoo and arm.

In addition to assessing the biocompatibility and interaction of SCs with ambient moisture, we examined the electrical response of the material to drying. Given that SCs are composed of salt and water, it is crucial to determine whether their exposure to air might cause the tattoos to dry out and lose their electrical functionality. To test this, six pairs of SC tattoos were created and exposed to the atmosphere in a non-air-controlled room at the same time. At specific intervals (0, 2, 4, 6, 8, and 24 h), a pair of SC tattoos was used to measure an ECG signal. After 24 h, one pair of electrodes was rehydrated by placing the SC tattoos face down in a Petri dish of tap water for 5 min before being utilized for ECG readings. ECG measurements were obtained and analyzed as stated previously, with the results presented in Figure S10. The SNR value was 110 ± 30 at 0 h, 65 ± 27 at 2 h, 76 ± 28 at 4 h, 67 ± 23 at 8 h, and 69 ± 23 at 24 h, indicating that exposure to an ambient environment causes a slight decrease in the SNR of ECG signals recorded with the SC tattoos. Notably, the SNR drops significantly after 2 h but stabilizes

over the next 16 h. However, the lower SNR values remain within one standard deviation of the original SNR for SCs (82 ± 24). Each measurement exhibited distinct ECG signal characteristics (P, Q, R, S, T), ensuring clear signal shape and information. Rehydrating the SCs after 24 h for 5 min resulted in an SNR of 75 ± 32, a value slightly higher than the 24 h measurement without rehydrating. The primary benefit of rehydration was restoring the tattoo's flexibility. After 24 h, the tattoos became stiff and brittle, but soaking them in water returned the material's pliability, facilitating easier handling without breakage.

EOG represents electrical signals similar to EMG signals but instead of recording muscle contractions, they are capturing the polarization of the eye's cornea and retina during ocular movements. For EOG recordings, the following two-pair electrode placement scheme was used: one electrode pair was positioned above and below the right eye, and one electrode pair was placed on the left and right temples. The electrodes above and below the eye were differentially connected to one channel, while those on the sides of the eyes were differentially connected to a separate channel. Such configuration enables the capture of electrical potentials arising from cornea-retina depolarization events accompanying eye movements. Figure 4C illustrates data obtained from the electrodes during a series of slow and controlled vertical eye movements (center-up-center-down-center), while Figure S11 showcases readings during a series of slow and controlled horizontal eye movements (center-left-center-right-center). As seen from these time traces, gazing horizontally creates a distinct reading in the appropriate horizontal channel of the EOG signal, while gazing vertically causes noticeable patterns recorded by the vertical electrode pair. These sharp signals make clear the gazing patterns performed. Notably, both gel electrode and SC tattoo measurements exhibit ''overshoot'' signals, attributed to the eyes returning from peripheral positions to the center. However, these overshoots provide valuable insights into specific eye movements, facilitating the differentiation and tracking of ocular positions during dynamic eye movement scenarios. While the signals received from the electrodes non-adjacent to the direction of testing (e.g., horizontal electrodes during vertical eye movements) show no major changes in signal amplitude, there are slight jumps in power during eye movements. A comparative analysis between SCs and Ag/AgCl gel electrodes reveals that both modalities effectively capture and present discernible and informative EOG signals.

EMG represents a potent electrical indicator closely associated with the physical contraction of muscles within the human body. When employing a differential electrode configuration, wherein two differential electrodes are positioned at each end of a muscle, the contraction of the muscle generates an electric potential. In the context of recording EMG signals, a pair of electrodes was placed on the anterior side of the subject's forearm, while an RE was placed on the nearby elbow. The subject executed a set of forearm contractions, utilizing both SCs and Ag/AgCl gel electrodes. The forearm contractions were readily discernible through the monitoring of EMG activity and the corresponding peaks in signal power. It is observed that the signal power of both the SCs and gel electrodes are roughly equivalent, differing from the increased signal amplitude of the ECG recordings. Notably, while the time trace derived from the gel electrodes exhibits less noise than the SCs, it remains evident, as depicted in Figure 4D, that the specific muscle movements and electrical signals are well distinguishable.

## Self-healing properties

Along with electrophysiological properties, SCs have the inherent property of self-healing due to their dough-like consistency and composition of water and salt. This composition will allow the creation of wearable technology that can resist damage to electrodes via self-healing. Here, the self-healing capability of SCs was tested by utilizing an SC tattoo as a resistor in a light-emitting diode (LED) circuit, as shown in Figure 5A. The resistance was measured using a commercial ohmmeter while simultaneously having a signal passed through the circuit. The resistance of the SC was measured before being cut in half, while being cut in half, and after being reconnected. Before being cut, the resistance of the SC was measured between 615 and 630 Ω with an average of 626 Ω while experiencing a 10 mA current. The SC was then cut in half using a plastic knife, disconnecting the circuit and causing the light-emitting diode (LED) to turn off. As expected, a massive increase in resistance was observed across the SC at a value around 57 MΩ. After 90 s, the two halves of the SC were gently reconnected, resulting in the reactivation of the LED. As predicted, the resistance of the SC returned to similar values as before the cut, with an average resistance of 623 Ω being recorded. This is due to the movement of the ions and water molecules returning to normal after being halted during disconnection, as shown in Figure 5B. Slight physical deformations existed near the center of the SC after reconnection due to the physical forces required for self-adhesion, but these deformations do not seem to impact the resistance of the material. These results prove the capabilities of SCs' self-healing, a property not seen in standard gel electrodes. This quality will open adjacent areas of research based on the creation of electrodes capable of withstanding significant physical forces and deformations.

## Temperature sensing

In a continued effort to expand the functionality of SCs, the electrodes were tested for their temperature-sensing abilities. This property broadens the potential applications of these circuits, as temperature monitoring is a vital component of wearable technologies. Temperature tracking will allow for an early indication and response to possible diseases and infections. To test the SCs' temperature-sensing capabilities, a piece of SC was placed on a hot plate and heated from room temperature to 65°C, then left to cool back down to room temperature. Temperature values were recorded using a commercial thermometer to monitor surface temperatures. Here, it was observed that the resistance of SCs is inversely proportional to the temperature of the thermometer. As seen in Figures 5C and 5D, the SCs feature a negative temperature electrical coefficient (TEC) with a coefficient of −0.014 during heating and −0.015 during cooling. The SCs behave similarly to Ag/AgCl gel electrodes, which also decrease in resistance with increasing temperature. During testing, the temperature increased in a stepwise fashion, increasing by 10°C every 30 min. The path of the resistance curve follows this trend inversely, decreasing in a stepwise fashion every 30 s. At 60°C, the minimum resistance was found at a value of around 3.5 kΩ. The max resistance was found when the temperature was at room temperature, with a

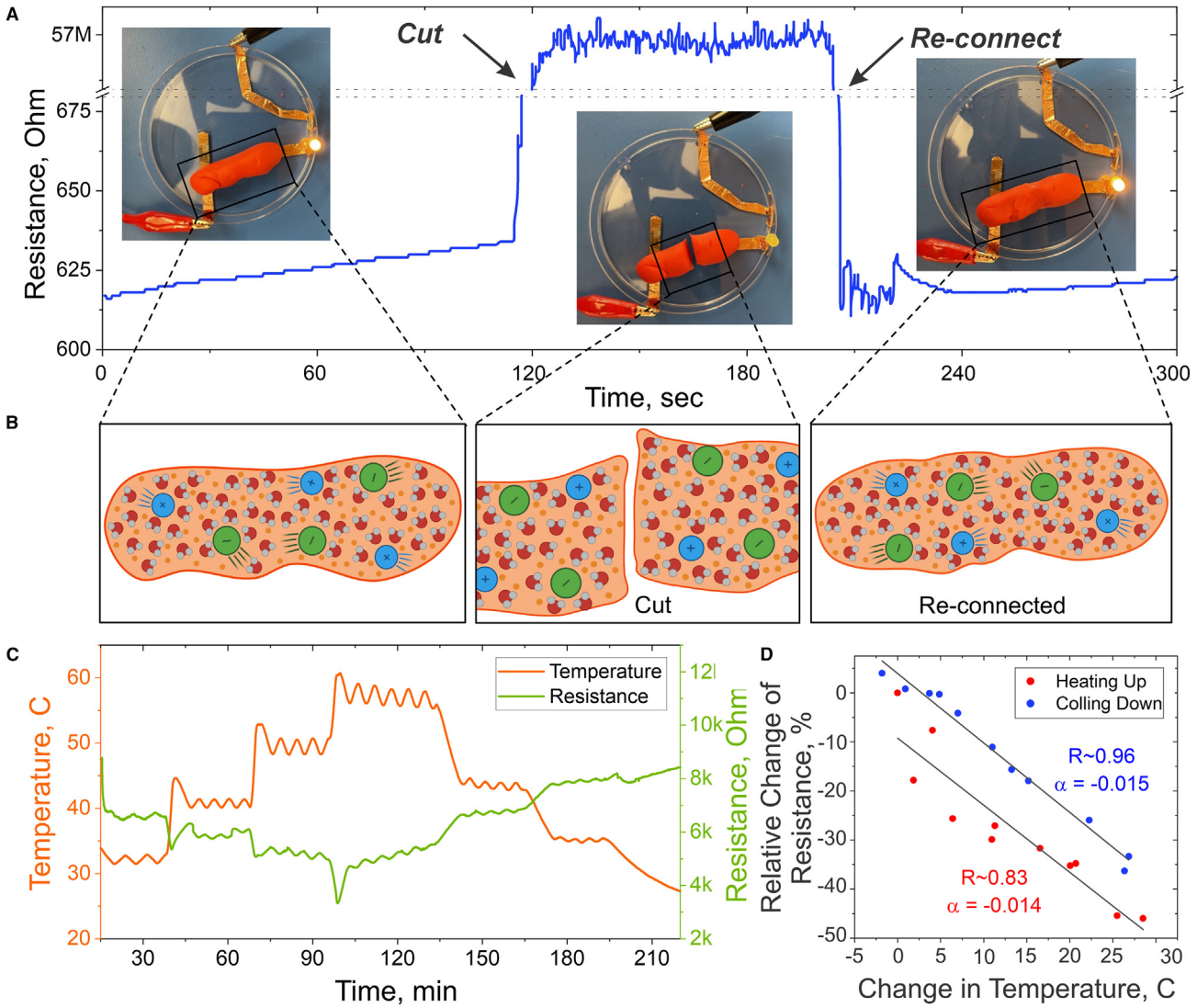


**Figure 5. Advanced properties of SCs for wearable applications**

(A) Resistance measurements taken while testing the self-healing properties.

(B) Schematic representation of the ionic flow within conductive SCs before being cut, when it is cut, and after being reconnected, demonstrating its self-healing properties.

(C) The plot of temperature (orange) and resistance (green) versus time taken for the temperature-sensing properties.

(D) Plot depicting the relationship between the change in temperature and relative change in resistance, both while heating up and cooling down. The line of best fit for heating and cooling has been overlaid onto the graph, with alpha values labeled.

value of 8.5 kΩ. It can be observed that there is no lag time in the change of resistance's response to a change in temperature, meaning the SCs immediately recognize and react to temperature changes due to innate material properties. It is important to note that the temperature sensing is performed in a uniquely different setup from the electrophysiological monitoring, and the temperature-related changes do not affect the quality or noise during EEG, ECG, EMG, and EOG sensing.

## Conclusions

In synthesizing these findings, our work not only explains the technical intricacies of SCs but also paves the way for their bioelectronic applications as low-cost wearables for various biomedical applications. SCs, crafted from low-cost household materials, not only provide an affordable alternative to traditional electrodes but also showcase superior functionalities. A typical SC-based electrode comes at a cost of ~$0.01 and is 25 times more effective compared even to mass-produced low-cost commercial gel electrodes. Our study reveals that SCs exhibit low impedance and high electrophysiological performance comparable to, or better than, commercial Ag/AgCl gel electrodes in EEG, ECG, EMG, and EOG measurements. Notably, SCs demonstrated a significantly lower impedance across a broad frequency spectrum, underscoring their potential for improved

signal quality in bioelectronic applications. Additionally, the intrinsic self-healing properties of SCs contribute to their durability and robustness, allowing them to maintain functionality under physical stress. The temperature-sensing capability of SCs further broadens their applicability in wearable technology, providing a responsive tool for monitoring physiological changes. These findings suggest that SCs could serve as a highly effective platform in the development of next-generation wearable bioelectronics, offering both cost efficiency and superior performance.

## EXPERIMENTAL PROCEDURES

### SCs

For this work, we have used the commercially pre-made SC dough. The dough is made by mixing flour (355 mL), water (237 mL), salt (59 mL), cream of tartar (44 mL), vegetable oil (15 mL), and food coloring, and the full step-by-step procedure can be found in Peppler et al.[24] and Conductive Play Dough – Salt Dough Recipe.[25]

### SC tattoo fabrication

3M Micropore Silicone Tape was cut into a 50 × 50 mm square. A horizontal 10 mm cut was made 15 mm from the top of the piece. 5-mm-wide copper tape was cut into a 40-mm-long strip. 15 mm of the liner was peeled, exposing the adhesive side of the copper tape. The copper was pushed through the cut, with the 15 mm of the adhesive face attached to the tape's adhesive side, while the other end remained on the non-adhesive side, creating a lead-out wire. A small amount of purple SC dough was rolled into a ball with a diameter of 1 cm. The ball was pressed into a 1-mm-thick disk via a 3D-printed stamper. The disk was then cut into a 25 × 20 mm rectangle to mimic the shape of the Cardinal Health Kendall 5400 Diagnostic Tab Electrodes. The SC rectangle was placed onto the tape. The exposed copper strip was centered to the rectangle, with the long direction of the copper parallel to the 25 mm direction of the electrode. The SC was lightly pressed into the tape to ensure adhesion while avoiding deformation. The tattoo was then placed on the skin SC-side down, allowing the silicone tape to adhere to the skin. Tattoos were connected to the Ganglion board via twisted pair cables connected to the lead-out copper wire.

### Skin impedance

Skin interface impedance was measured in 2-probe and 4-probe configurations via a Hioki LCR meter IM 3536 (see Figure S12 for configuration). The frequency sweep range was set to 10 Hz–1 MHz. The measurements were performed with a constant current mode with 0.05 V and 1 mA alternative current amplitude without direct current bias. Each test was measured three times with a 5 s interval between sweeps. Green SCs were measured against 3M Red Dot and Medline MedGel gel electrodes. SC tattoos were made with the dimensions of 25 × 20 mm to match the gel electrode sizes. The human skin tests were performed on one subject to eliminate any variability due to multiple subjects. The porcine skin was stored in a frozen state, thawed (in 4°C fridge) 24 h prior to the experiment, and tested at room temperature. Paper towels were used to dry off the skin and ensure that little to no moisture or water was present on the skin to interfere with testing. Skin moisture was not monitored or manually changed/induced during tests. All acquired data were graphed and analyzed on OriginPro.

### EIS

Working electrodes were constructed by adhering a strip of copper tape (5 × 60 mm) onto a glass slide, forming the electrode surface. Various 3D open-ended plastic cylinders and cones of differing sizes were attached to this surface (diameters of 10, 7.5, and 5 mm). Each plastic cylinder was adhered to the surface using polydimethylsiloxane (PDMS; Sylgard 184); the PDMS precursor was made by mixing the base and curing agent in ratio of 10:1 (w/w), to hold the liquid electrolyte. The thickness of the green SC studied remained constant at 2 mm throughout the experiments. Copper tape and 3M Red Dot gel electrodes were used as control measurements. The PalmSens 4 Potentiostat with PSTrace software was utilized for data collection and processing for EIS analysis. The experimental setup featured a standard electrolyte solution of 1×PBS (Sigma-Aldrich), with an Ag/AgCl used as an RE, a Pt wire as a counter electrode (CE), and the SC or control materials as the working electrode. The EIS was measured by sweeping the frequency from 1 Hz to 100 kHz. The areas utilized during the EIS tests were 78.54, 44.18, and 19.635 $mm^2$. All data acquired from the measurements was graphed and analyzed using OriginPro.

### Electrophysiology data analysis

Data analysis was performed via MATLAB. OpenBCI's Ganglion board was utilized to capture raw ECG, EMG, EEG, and EOG data. The recordings from the four channels were arranged and stored in four separate vectors. A 60 Hz notch filter was applied to all signals to remove powerline interference. A 4th-order Butterworth low-pass filter with a cutoff frequency of 50 Hz was applied to all ECG, EMG, and EOG signals to further cut off high-frequency noise. A high-pass filter with a cutoff frequency of 0.5 Hz was applied to the ECG signals to remove low-frequency breathing artifacts. To find the SNR for the ECG signals, a peak finding algorithm was utilized. The amplitudes of the differences between each R and S waves were found and averaged to find an average signal amplitude. To find the noise, regions between each P and T wave with a duration of 200 ms were extracted. The median absolute deviation of each region was found and averaged to find an average noise value. The SNR was calculated by dividing the signal amplitude by the noise value. For the EMG signals, a 20 Hz cutoff low-pass filter was implemented to eliminate motion artifacts due to muscle movement. The EEG recordings were recorded in the range of 320–360 s. Two of the four OpenBCI channels were connected to electrodes connected to the Fp1 and Fp2 locations of the 10–20 EEG system. Both were connected to a common RE on the earlobe. After the 60 Hz notch filter was implemented, a linear detrending was implemented to remove the baseline. Next, a 40 Hz cutoff low-pass filter was applied to reduce high-frequency noise. A STFT was then implemented with a Hamming window of 512 sample length and an Fast Fourier transform length of 512 samples. The STFT results consisted of a matrix of frequencies and time samples, Fourier coefficients, and power spectral densities in dB. These results were used for spectrogram plotting.

### Self-healing testing

Resistance measurements were collected using a Keysight B2902B Precision Source/Measurement Unit (SMU) and recorded using Quick IV software. A piece of orange SC was rolled out into a cylindrical shape and connected in series with an LED and the SMU via copper wires inserted into the SC. A constant current of 10 mA with a maximum voltage of 10 V was applied to the circuit. Resistance data were collected for 120 s before the SC was cut in half with a plastic knife. After 90 s, a small amount of physical pressure was applied to reconnect the two halves. Resistance measurements continued for 90 s after SC reconnection. The data were analyzed and graphed using OriginPro.

### Temperature-sensing testing

A 3D-printed mold (10 × 5 × 40 mm) was filled with orange SC and taped onto a hotplate. An Amprobe TMD-56 thermometer was utilized for temperature measuring. One of the thermometer's 2 channels was connected to the hotplate, while the other was connected directly to the SC, both attached via copper tape. The thermometer took measurements from both channels each second. A Keystone B2902B Precision SMU was connected in series to the SC to measure resistance. The Keystone B2902B was controlled via Quick IV software configured to a source and sample setting. The current was set to 100 μA, the compliance voltage to 10 V, and the source range to 100 μA. Data points were measured once per second. Resistance measurements started while the SC was at room temperature. After 10 min, the hot plate was set to 35°C. Every subsequent 30 min, the temperature of the hotplate was increased by 10°C to a maximum of 65°C. The temperature was then decreased to 50°C, then 40°C, and then room temperature, recording data at each temperature for 30 min. The data were analyzed and graphed in OriginPro.

## RESOURCE AVAILABILITY

### Lead contact

Further information and requests for resources should be directed to the lead contact, Dmitry Kireev (dkireev@umass.edu).

### Materials availability

This study did not generate new unique reagents. The SCs can be made accordingly to the official recipes.[24,25]

### Data and code availability

All data of this study are available within the article and supplemental information.

## ACKNOWLEDGMENTS

D.K. acknowledges the University of Massachusetts Amherst Startup funds. The authors acknowledge Prashant Narute for the discussion of the manuscript.

## AUTHOR CONTRIBUTIONS

D.K. conceptualized the work. A.K. performed the EIS experiments and analyzed corresponding data. F.N. performed human skin and porcine skin impedance experiments and analyzed corresponding data. M.M. performed self-healing and temperature-sensing experiments and analyzed corresponding data. S.M. performed wearable electrophysiology experiments and analyzed corresponding data. M.B. and O.T. performed resistance measurements and analyzed corresponding data. D.K. supervised the project and wrote the initial manuscript version. All authors contributed to the final version of the manuscript.

## DECLARATION OF INTERESTS

The authors declare no competing interests.

## DECLARATION OF GENERATIVE AI AND AI-ASSISTED TECHNOLOGIES IN THE WRITING PROCESS

During the preparation of this work, the authors used ChatGPT 4 in order to proofread the text, ensure readability, reducing duplicate statements, and help provide succinct summaries. The tool was not used to generate any information besides editing and summaries. After using this tool, the authors reviewed and edited the content as needed and take full responsibility for the content of the published article.

## SUPPLEMENTAL INFORMATION

Supplemental information can be found online at https://doi.org/10.1016/j.device.2024.100553.

Received: June 4, 2024
Revised: August 12, 2024
Accepted: August 16, 2024
Published: September 18, 2024

## REFERENCES

1. Rogers, J., Bao, Z., and Lee, T.W. (2019). Wearable Bioelectronics: Opportunities for Chemistry. Acc. Chem. Res. *52*, 521–522. https://doi.org/10.1021/acs.accounts.9b00048.
2. Sunwoo, S.H., Ha, K.H., Lee, S., Lu, N., and Kim, D.H. (2021). Wearable and Implantable Soft Bioelectronics: Device Designs and Material Strategies. Annu. Rev. Chem. Biomol. Eng. *12*, 359–391. https://doi.org/10.1146/annurev-chembioeng-101420-024336.
3. Kumari, P., Mathew, L., and Syal, P. (2017). Increasing trend of wearables and multimodal interface for human activity monitoring: A review. Biosens. Bioelectron. *90*, 298–307. https://doi.org/10.1016/j.bios.2016.12.001.
4. Someya, T., Bao, Z., and Malliaras, G.G. (2016). The rise of plastic bioelectronics. Nature *540*, 379–385. https://doi.org/10.1038/nature21004.
5. Kim, J., Campbell, A.S., de Ávila, B.E.F., and Wang, J. (2019). Wearable biosensors for healthcare monitoring. Nat. Biotechnol. *37*, 389–406. https://doi.org/10.1038/s41587-019-0045-y.
6. Li, H., Tan, P., Rao, Y., Bhattacharya, S., Wang, Z., Kim, S., Gangopadhyay, S., Shi, H., Jankovic, M., Huh, H., et al. (2024). E-Tattoos: Toward Functional but Imperceptible Interfacing with Human Skin. Chem. Rev. *124*, 3220–3283. https://doi.org/10.1021/acs.chemrev.3c00626.
7. Gong, S., Lu, Y., Yin, J., Levin, A., and Cheng, W. (2024). Materials-Driven Soft Wearable Bioelectronics for Connected Healthcare. Chem. Rev. *124*, 455–553. https://doi.org/10.1021/acs.chemrev.3c00502.
8. Zhu, Y., Wang, Z., and Ma, S. (2024). Low-cost wearable pulse monitor for AI-assisted cardiovascular healthcare. Device *2*, 100315. https://doi.org/10.1016/j.device.2024.100315.
9. Yang, T., Jiang, X., Zhong, Y., Zhao, X., Lin, S., Li, J., Li, X., Xu, J., Li, Z., and Zhu, H. (2017). A Wearable and Highly Sensitive Graphene Strain Sensor for Precise Home-Based Pulse Wave Monitoring. ACS Sens. *2*, 967–974. https://doi.org/10.1021/acssensors.7b00230.
10. Trung, T.Q., Ramasundaram, S., Hwang, B.U., and Lee, N.E. (2016). An All-Elastomeric Transparent and Stretchable Temperature Sensor for Body-Attachable Wearable Electronics. Adv. Mater. *28*, 502–509. https://doi.org/10.1002/adma.201504441.
11. Pang, Y., Yang, Z., Yang, Y., and Ren, T.L. (2020). Wearable Electronics Based on 2D Materials for Human Physiological Information Detection. Small *16*, e1901124–e1901126. https://doi.org/10.1002/smll.201901124.
12. Yin, J., Wang, S., Tat, T., and Chen, J. (2024). Motion artefact management for soft bioelectronics. Nat. Rev. Bioeng. *2*, 541–558. https://doi.org/10.1038/s44222-024-00175-4.
13. Wang, F., Zhang, C., and Wan, X. (2021). Carbon Nanotubes-Coated Conductive Elastomer: Electrical and near Infrared Light Dual-Stimulated Shape Memory, Self-Healing, and Wearable Sensing. Ind. Eng. Chem. Res. *60*, 2954–2961. https://doi.org/10.1021/acs.iecr.0c06050.
14. Kireev, D., Ameri, S.K., Nederveld, A., Kampfe, J., Jang, H., Lu, N., and Akinwande, D. (2021). Fabrication, characterization and applications of graphene electronic tattoos. Nat. Protoc. *16*, 2395–2417. https://doi.org/10.1038/s41596-020-00489-8.
15. Lim, C., Shin, Y., Jung, J., Kim, J.H., Lee, S., and Kim, D.-H. (2019). Stretchable conductive nanocomposite based on alginate hydrogel and silver nanowires for wearable electronics. Apl. Mater. *7*, 031502. https://doi.org/10.1063/1.5063657.
16. Ferrari, L.M., Sudha, S., Tarantino, S., Esposti, R., Bolzoni, F., Cavallari, P., Cipriani, C., Mattoli, V., and Greco, F. (2018). Ultraconformable Temporary Tattoo Electrodes for Electrophysiology. Adv. Sci. *5*, 1700771. https://doi.org/10.1002/advs.201700771.
17. Lim, K., Seo, H., Chung, W.G., Song, H., Oh, M., Ryu, S.Y., Kim, Y., and Park, J.-U. (2024). Material and structural considerations for high-performance electrodes for wearable skin devices. Commun. Mater. *5*, 49. https://doi.org/10.1038/s43246-024-00490-8.
18. Ates, H.C., Nguyen, P.Q., Gonzalez-Macia, L., Morales-Narváez, E., Güder, F., Collins, J.J., and Dincer, C. (2022). End-to-end design of wearable sensors. Nat. Rev. Mater. *7*, 887–907. https://doi.org/10.1038/s41578-022-00460-x.
19. Xu, Y., Zhao, G., Zhu, L., Fei, Q., Zhang, Z., Chen, Z., An, F., Chen, Y., Ling, Y., Guo, P., et al. (2020). Pencil-paper on-skin electronics. Proc. Natl. Acad. Sci. USA *117*, 18292–18301. https://doi.org/10.1073/pnas.2008422117.
20. Ershad, F., Thukral, A., Yue, J., Comeaux, P., Lu, Y., Shim, H., Sim, K., Kim, N.-I., Rao, Z., Guevara, R., et al. (2020). Ultra-conformal drawn-on--skin electronics for multifunctional motion artifact-free sensing and point-of-care treatment. Nat. Commun. *11*, 3823. https://doi.org/10.1038/s41467-020-17619-1.
21. Patel, S., Ershad, F., Lee, J., Chacon-Alberty, L., Wang, Y., Morales-Garza, M.A., Haces-Garcia, A., Jang, S., Gonzalez, L., Contreras, L., et al. (2022). Drawn-on-Skin Sensors from Fully Biocompatible Inks toward High-Quality Electrophysiology (Small 36/2022). Small *18*, 2270194. https://doi.org/10.1002/smll.202270194.

22. Zhang, Y.-Z., Lee, K.H., Anjum, D.H., Sougrat, R., Jiang, Q., Kim, H., and Alshareef, H.N. (2018). MXenes stretch hydrogel sensor performance to new limits. Sci. Adv. *4*, eaat0098. https://doi.org/10.1126/sciadv.aat0098.

23. Zou, Z., Zhu, C., Li, Y., Lei, X., Zhang, W., and Xiao, J. (2018). Rehealable, fully recyclable, and malleable electronic skin enabled by dynamic covalent thermoset nanocomposite. Sci. Adv. *4*, eaaq0508. https://doi.org/10.1126/sciadv.aaq0508.

24. Peppler, K., Wohlwend, K., Thompson, N., Tan, V., and Thomas, A. (2019). Squishing Circuits: Circuitry Learning with Electronics and Playdough in Early Childhood. J. Sci. Educ. Technol. *28*, 118–132. https://doi.org/10.1007/s10956-018-9752-2.

25. Conductive Play Dough - Salt Dough Recipe. https://squishycircuits.com/pages/salt-dough-recipe-conductive-play-dough.

26. Simini, F., and Bertemes-Filho, P. (2018). Bioimpedance in Biomedical Applications and Research (Springer International Publishing). https://doi.org/10.1007/978-3-319-74388-2.

27. Sel, K., Osman, D., and Jafari, R. (2021). Non-Invasive Cardiac and Respiratory Activity Assessment From Various Human Body Locations Using Bioimpedance. IEEE Open J. Eng. Med. Biol. *2*, 210–217. https://doi.org/10.1109/OJEMB.2021.3085482.

28. Sel, K., Kireev, D., Brown, A., Ibrahim, B., Akinwande, D., and Jafari, R. (2019). Electrical Characterization of Graphene-based e-Tattoos for Bio-Impedance-based Physiological Sensing. In 2019 IEEE Biomedical Circuits and Systems Conference (BioCAS) (IEEE), pp. 1–4. https://doi.org/10.1109/BIOCAS.2019.8919003.

29. Matthie, J.R. (2008). Bioimpedance measurements of human body composition: Critical analysis and outlook. Expet Rev. Med. Dev. *5*, 239–261. https://doi.org/10.1586/17434440.5.2.239.

30. Narayan, R. (2022). Encyclopedia of Sensors and BiosensorsFirst Edition, *Volume 1–4*.

31. Becq, G., Bienkowski, G., Diard, J.P., and Villard, C. (2008). About MEA impedance measurement and analysis. In 6th International Meeting on SubstrateIntegrated Micro Electrode Arrays, pp. 277–278.

32. Boehler, C., Carli, S., Fadiga, L., Stieglitz, T., and Asplund, M. (2020). Tutorial: guidelines for standardized performance tests for electrodes intended for neural interfaces and bioelectronics. Nat. Protoc. *15*, 3557–3578. https://doi.org/10.1038/s41596-020-0389-2.